RSC Advances

ROYAL SOCIETY OF CHEMISTRY

www.rsc.org/advances

ARTICLE TYPE www.rsc.org/xxxxxx | XXXXXXXX

High-Active Direct Z-scheme Si/TiO_2 Photocatalyst for Boosted CO_2 Reduction into Value-added Methanol

Yousong Liu [a], Guangbin Ji [a]*, Mohammed Abdulkader Dastageer [b], Lei Zhu [a], Junyi Wang [a], Bin Zhang [a], Xiaofeng Chang [a] and Mohammed Ashraf Gondal [b]*

Received (in XXX, XXX) Xth XXXXXXXXX 200X, Accepted Xth XXXXXXXXX 200X
DOI: 10.1039/b000000x

In the present study,direct Z-scheme Si/TiO_2 photocatalyst was synthesized via a facile hydrothermal reaction using tetrabutyl titanate and Si powder prepared from the magnesiothermic reduction of SiO_2 nanospheres. The Si/TiO_2 nanospheres were composed of porous Si nanospheres with a diameter of ~300 nm and TiO_2 nanosheets with the diameter of 50 nm and thickness of 10 nm, and demonstrated superior visible light harvesting ability to either Si nanospheres or TiO_2 nanosheets. CO_2 photocatalytic reduction proved that Si/TiO_2 nanocomposites exhibit high activity in conversion of CO_2 to methanol with the maximum photonic efficiency of 18.1%, while pure Si and TiO_2 catalyst are almost inactive, which can be ascribed to the integrated suitable band composition in the Si/TiO_2 Z-scheme system for CO_2 reduction. The enhanced photocatalytic property of Z-scheme Si/TiO_2 nanospheres was ascribed to the formation of Si/TiO_2 Z-scheme system, which improved the separation efficiency of the photo-generated carries, prolonged their longevity, and therefore boosted their photocatalytic activity.

1. Introduction

High consumption of fossil fuels brings about not only the energy crisis but also the environmental pollution and climate change due to the excessive green house gas emissions to the atmosphere. As carbon dioxide (CO_2) is a major contributor to green house gases, more attention is focused on its mitigation all over the world. Solar-driven photocatalytic conversion of CO_2 into added value fuels is the most promising proposition as it does not only remove CO_2 from effluent gases but also produces hydrocarbon fuels, which could be used to meet the future energy needs. Thus， a lot of research efforts have been focused on developing the efficient catalysts for CO_2 photocatalytic reduction. Semiconductor photocatalysts (such as ZnO,[1, 2] CdS, [3] $ZnGa_2O_4$,[4] Zn_2GeO_4 ,[5-6] WO_3 ,[7] TiO_2 [8] etc.) have been explored. Among them, titanium dioxide (TiO_2) was extensively studied as an important photocatalyst because of its nontoxicity, low cost, superior photocatalytic activity and long-term chemical stability .[9-11] However, the wide band gap of TiO_2 (~3.2 eV) limits its efficient utilization for solar energy conversation as TiO_2 only absorbs the light with wavelength shorter than ~387 nm in the ultraviolet region. Moreover, after the photo-absorption, the electrons are excited from the valence band of TiO_2 to the conduction band and the effective electron-hole pairs are generated.[12] Unfortunately, most of the effective electron-hole pairs are recombined and dissipated as heat before they arrive at the photocatalyst surface, which makes TiO_2 as inefficient photo-generated carrier and hampers its charge separation ability.

Research scientists have devoted extensive efforts to address these problems. Introducing doping elements (such as S,[13] N,[14] and C[15]) into TiO_2 has been proved to be an effective approach to narrow the band gap, improve the visible light absorption and enhance the photocatalytic activity in CO_2 reduction. TiO_2 modification with metal particles (e.g. Ag,[16] Au,[17] Pt,[18] and Cu[19]) has been reported to inhibit charge recombination probability because these metals served as electron traps to suppress the recombination of the photo-generated electron-hole pairs and hence improve the photocatalytic activity. In addition, coupling TiO_2 with a narrower band gap semiconductor to construct heterojunction is another effective approach to accommodate the visible-light photon energy and improve the photo-generated charge separation, and CO_2 conversion efficiency by taking advantage of both the heterojunction to improve charge separation rate and narrow band gap of coupled semiconductor to expand light absorption region. TiO_2 based heterojunctions such as PbS/TiO_2,[20] CuO/TiO_2,[21] $FeTiO_3$/TiO_2 [22] have been reported in recent years.

Similar to the heterojunction photocatalytic system, the Z-scheme photocatalytic system also feagures the spatial isolation of photogenerated electrons and holes, which reduces the bulk electron-hole recombination[23]. However, Z-scheme photocatalytic system is generally constructed by employing conductor as the electron mediator to form the known Ohmic contact with low contact resistance. Until now, many Z-scheme systems have been reported, such as TiO_2-Au-CdS system,[24] AgBr-Ag-AgI,[25] and ZnO-Au-CdS,[26] etc. Recently, studies on the direct Z-scheme photocatalysts (such as g-C_3N_4-TiO_2 and WO_3-$NaNbO_3$ system) have been investigated for photocatalytic water splitting, CO_2 conversion and photocatalytic decomposition[27-29].

A narrow band gap semiconductor, silicon (1.12 eV) has

drawn considerable interest because of its potential application in optoelectronic devices and integrated microelectronics. Recently, studies of silicon materials have reported its promising photocatalytic activity. Shao *et al*. prepared hydrogen-terminated Si nanowires (Si NWs) and noble metal-modified (Pt, Pd, Au, Rh, Ag) Si NWs substrates by oxide-assisted growth method and investigated their performance for the degradation of Rhodamine B and oxidation of benzyl alcohol to benzoic acid under visible light irradiation.[30] Independently, Megouda *et al*. investigated the performance of hydrogen-terminated Si NWs and two kinds of metals (Ag, Cu) decorating Si NWs for the degradation of dye molecules.[31] Furthermore, literatures about Si/TiO_2 heterojunction to achieve enhanced photochemical and photocatalytic properties have been reported.[32] Wang *et al*. successfully deposited TiO_2 onto Si nanowire arrays to construct Si/TiO_2 heterojunction using a surface reaction-limited pulsed chemical vapor deposition method and tailor electrical properties of TiO_2 for wider spectrum solar energy havesting and conversion.[33] Li *et al*. attained a novel composite material of TiO_2 and porous silicon using a sol-gel method and found that it exhibits much higher photocatalytic activity for the degradation of RhB.[34] Recently, direct Z-scheme Si/TiO_2 tree-like heterostructure was constructed by Yang [35], which is demonstrated to greatly improve the photocatalytic activity of H_2 evolution. Research on the direct Z-scheme system is just a recent work, and still needs further study.

In this work, we report a novel direct Z-scheme Si/TiO_2 photocatalyst synthesized via a facile hydrothermal method with tetrabutyl titanate and Si powder prepared from the magnesiothermic reduction of SiO_2 stöber nanospheres[36]. The enhanced photocatalytic conversion of CO_2 reduction into value-added methanol was investigated.

2. Experimental section

2.1 Synthesis of SiO_2 nanospheres

The mono-disperse silica spheres were prepared by hydrolysis and condensation of tetraethoxysilane (TEOS) in a mixture of water, ammonia, and ethanol. In a typical synthesis process, 9 mL 28wt% ammonia water was mixed with 16.25 mL ethanol and 24.75 mL deionized water under a stirring condition (solution A). 4.5 mL TEOS was added to 45.5 mL ethanol under stirring (solution B). Here, we added B to A drop by drop and strewed for another 2 h at room temperature. SiO_2 nanospheres were centrifuged from the mixture, alternately washed with deionized water and ethanol for 3 times and then dried at 100 ^oC for 12 h.

2.2 Synthesis of Si nanospheres

0.5 g SiO_2 nanospheres and 0.42 g Mg powder were ground for 5 minutes and then transferred into a crucible to calcine at 750 ^oC for 5 h under N_2 atmosphere. After cooling to the room temperature, the powder was then added to 50 mL 32wt% HCl solution under stirring for 24 h. Si nanospheres were then cleaned several times by centrifugation and water dispersion and finally dried into powders at 60 ^oC in a vacuum oven for 12 h.

2.3 Synthesis of Direct Z-scheme Si/TiO_2 nanospheres

Direct Z-scheme Si/TiO_2 nanospheres were fabricated via a facile hydrothermal reaction with tetrabutyl titanate and Si nanospheres. In a typical process, 25 mL of $Ti(OBu)_4$ and 1.5 g Si nanospheres were added in a 100 mL Teflon pot and 3 mL of hydrofluoric acid was added dropwise under stirring. After stirring for 15 min at room temperature, the Teflon pot was sealed and kept at 200 ^oC for 24 h. Finally, the as-prepared Si/TiO_2 nanospheres were obtained after the resulting precipitate was centrifuged for three times, washed with ethanol to remove the hydrofluoric acid and organics, and then dried in a vacuum oven for 12 h. Pure TiO_2 sample was prepared in a same hydrothermal reaction without Si nanospheres.

2.4 Characterizations

The crystal structure of all the samples was examined by means of X-ray diffraction analysis (XRD, Bruker D8 ADVANCE with Cu-Kα radiation, λ=1.5418 Å). The morphology and particle size were determined by a field emission scanning electron microscopy (FE-SEM, Hitachi S4800) and transmission electron microscopy (TEM, JEOL JSM-2010) with an accelerating voltage of 200 kV. UV-Vis absorption spectra were obtained using a UV-Vis spectrometer (Shimadzu UV-3600). Photoluminescence (PL) spectra were obtained with an Edinburgh Instrument FLS 920 spectrometer. The excitation wavelength λ_{ex} was 360 nm, and both the bandwidths of excitation and emission were 5 nm. The Brunauer-Emmet-Teller (BET) specific surface area of the samples were determined by a high speed automated area and pore size analyzer (ASAP 2010).

2.5 Photocatalytic reduction of CO_2 under 355 laser irradiation

The photo-catalytic reaction cell and its setup have been described in our earlier publication[37]. The photo-catalytic reactor is cylindrical stainless steel cell with quartz windows on the top to enable the transmission of 355 nm pulse laser radiations. At the bottom of the cell there is a gas inlet with a needle valve which lets the CO_2 gas pass through the distilled water in the cell and there is an outlet fixed with the rubber septum in order to dispense the sample through the syringe almost at the same level at the opposite side. The whole cell is kept on a magnetic stirrer that constantly replenishes the photo-catalyst in the path of laser radiations. Care has been taken not to let the water level to go very much higher than the level of the catalyst platform in order to have better interaction of radiation with the photocatalyst. Since the quantity of sample taken for gas chromatographic analysis at each time was around 4.0 μL, the water level did not decrease due to sample withdrawing from the reaction cell. The reaction cell was cleaned, dried, then was tightly closed and checked for leaks up to 50 psi pressure after 1.0 g catalyst was loaded along with 100 mL distilled water. High purity CO_2 gas (99.99%) was introduced through reactor inlets and the reactor pressure

was maintained at 50 psi. Prior to turning on the pulsed laser, CO_2 gas was purged into 100 mL water containing 1.0 g catalyst for 30 min in order to saturate the contents of the reactor with CO_2. After a predetermined irradiation time, water samples were withdrawn from the reactor using syringe without opening the reactor and subjected to GC analysis.

The laser (wavelength = 355 nm) used for this study was the third harmonic of the pulsed Nd:YAG laser (Model Spectra Physics GCR 250-10) operated at 10 Hz and the pulse width of ~8 ns. Throughout this study, laser pulse energy of 40 mJ was used. The laser beam was routed with the high power UV reflecting mirrors/dichroic mirrors so that the beam enters from the top of the cell and appropriate lens was also used to slightly expand the beam to the same diameter of the catalyst platform when it reaches there. Although the laser pulse energy was quite stable it was monitored throughout the experiment with the 50-50 beam splitter and the laser energy meter supplied by Coherent USA.

The water samples were analyzed for methanol and other hydrocarbons using gas chromatograph equipped with flame ionization detector (FID). The components separation was carried out on Rtx-Wax column (dimensions: 30 m x 0.32 mm x 0.32 mm) obtained from Restek, using temperature programmed conditions. For the analysis of end products, 4.0 µL of the laser irradiated sample was injected into the gas chromatograph and the operating conditions were as follows: Oven temperature was set at 40 ^oC which was then increased to 90 ^oC at 5 ^oC/min heating rate and increased to 180 ^oC at the rate of 50 ^oC/min to elute all the components from the column before injecting another sample. The injector and detectors were both set at 200 ^oC and helium was used as carrier gas. The total analysis run time was 11.8 min. A calibration plot was established for methanol standard solution in distilled water for calculating the amount of methanol produced as a function of irradiation time.

2.6 Photocatalytic Reduction of CO_2 under Xe arc lamp irradiation

In a typical process, 0.1 g of the samples was uniformly dispersed on the glass reactor (4.2 cm^2). A 300 W Xenon arc lamp was used as the light source. The reaction system (230 mL in volume) was vacuum-treated several times, and then the high purity of CO_2 gas was followed into the reaction setup for reaching ambient pressure. 0.4 mL of deionized water was injected into the reaction system as reducer. The as-prepared photocatalysts were allowed to equilibrate in the CO_2/H_2O atmosphere for several hours to ensure that the adsorption of gas molecules was complete. During the irradiation, about 1 mL of gas was continually taken from the reaction cell at given time intervals for subsequent CH_4 concentration analysis by using gas chromatograph (GC-2014, Shimadzu Corp., Japan). All samples were treated at 300 ^oC in nitrogen atmosphere for 2 h for removal of organic adsorbates before the photocatalysis reaction.

2.7 Photocatalytic degradation of aqueous RhB solution

The photocatalytic activity was measured as follows: 0.100 g of as-prepared TiO_2 and Si/TiO_2 samples were added to a 250 mL Pyrex glass vessel which contained 200 mL RhB solution (7.5 mg/L). The light source was a 300 W Xe arc lamp (CHF-XM500W, Beijing TrustTech Co. Ltd.) with an illumination intensity of 400 mW/cm^2. Prior to irradiation, RhB solution suspended with photocatalysts was stirred in the dark for 30 min to ensure that the surface of photocatalysts reaches the adsorption-desorption equilibrium. 3 mL of the suspension was withdrawn throughout the experiment after every 10 min. The samples were analyzed by a UV-Vis spectrophotometer after removing the catalyst powders by centrifugation.

3. Results and discussion

3.1 Phase and morphology analysis

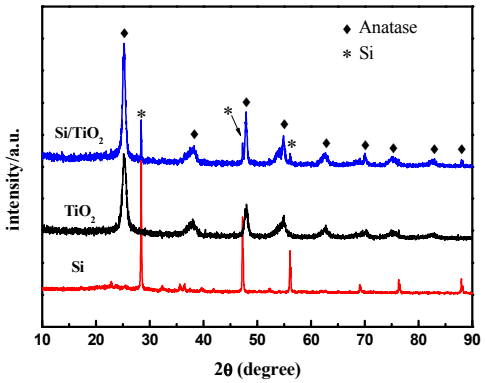

Figure 1. XRD patterns of the as-prepared Si nanospheres, TiO_2 nanosheets and direct Z-scheme Si/TiO_2 nanospheres.

The X-ray diffraction patterns of as-prepared Si nanospheres, TiO_2 nanosheets and direct Z-scheme Si/TiO_2 nanospheres are depicted in Figure 1. The diffraction peaks in the XRD curve marked in red at 28.4 °, 47.3 °, 56.1 °, 69.1 °, 76.3 ° and 88.0 ° can be assigned to (111), (220), (311), (400), (331) and (422) planes of Si (JCPDS Card 27-1402), respectively. The narrow broadness of diffraction peaks for Si nanospheres indicates that the Si nanospheres prepared via a magnesiothermic reduction method have a high purity and crystallinity. The diffraction peaks in the XRD curve marked in black at 25.3 °, 37.8 °, 48.0 °, 55.0 °, 62.6 °, 70.3 °, 75.0 ° and 82.1 ° are indexed to the (101), (004), (200), (211), (204), (220), (215) and (303) planes of TiO_2 (JCPDS Card 21-1272), respectively. From the diffraction peaks in the XRD curve of direct Z-scheme Si/TiO_2 nanospheres marked in blue, which contain both the Si and TiO_2 diffraction peaks, it can be seen obviously that the Si/TiO_2 product obtained via a hydrothermal method is composed of Si and TiO_2. The diffraction peaks of Si in the XRD curve of direct Z-scheme Si/TiO_2 nanospheres are very low, which may be resulted from its low content.

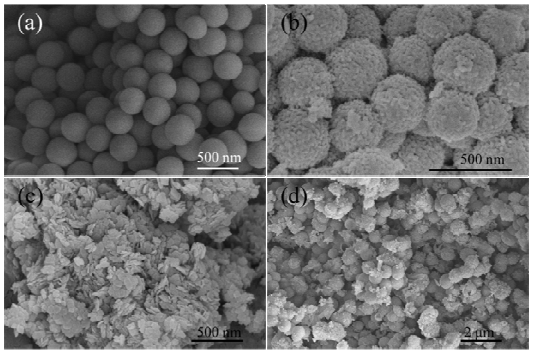

Figure 2. SEM images of as-prepared SiO_2 nanospheres (a), Si nanospheres (b), TiO_2 nanosheets (c), and direct Z-scheme Si/TiO_2 nanospheres (d).

As depicted in Figure 2(a), the SiO_2 nanospheres prepared via the Stöber method are monodisperse and uniform with a smooth surface and an average diameter of about 300 nm. After the magnesiothermic reduction process, Si nanospheres were obtained with a porous structure and rough surface, resulted from the loss of O atoms from SiO_2 nanospheres captured by Mg under high temperature. The diameter of Si nanospheres remained unchanged approximately (as shown in Figure 2(b)). The SEM images of the contrast TiO_2 samples prepared by a hydrothermal method without adding Si nanospheres are depicted in Figure 2(c). It can be seen that the TiO_2 nanoparticles displayed a uniform sheet shape with an average edge length of about 100 nm and a thickness of about 10 nm. Figure 2(d) shows the representative SEM image of direct Z-scheme Si/TiO_2 nanospheres, clearly indicating the Si nanospheres were coated with TiO_2 nanosheets.

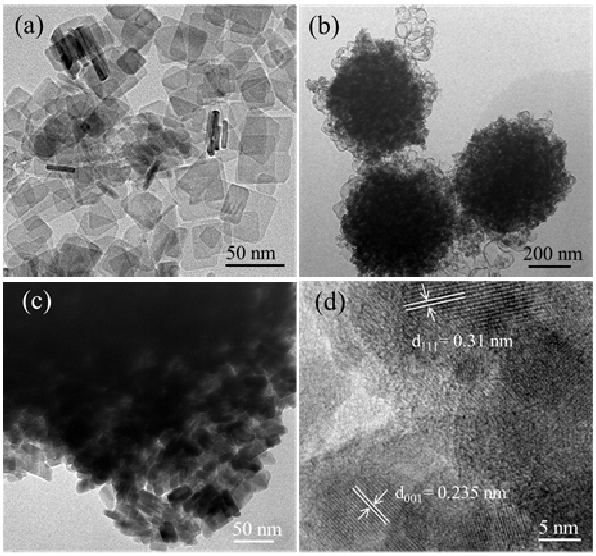

Figure 3. TEM images: (a) TiO_2 nanosheets, (b, c) direct Z-scheme Si/TiO_2 nanospheres, (d) high-magnification TEM image of direct Z-scheme Si/TiO_2 nanospheres.

In order to obtain further information on the structure of the samples, TEM observation of the TiO_2 nanosheets and direct Z-scheme Si/TiO_2 nanospheres was carried out. It can be clearly noticed from Figure 3(a) that the as-prepared TiO_2 samples are composed of large quantity of square nanosheets with an average edge length of about 100 nm and a thickness of about 10 nm, which is in good agreement with the result obtained from the SEM images. The TEM image of Si/TiO_2 direct Z-scheme nanocomposites in Figure 3(b) clearly shows that the Si nanospheres were coated by TiO_2 nanosheets. Moreover, it can be observed that the Si nanospheres appear a porous morphology resulted from the O element captured by Mg in the magnesiothermic reduction process. The magnified TEM image of the nanostructure of the Si/TiO_2 nanocomposites in Fig. 3(c) presents the TiO_2 nanosheets aggregation morphology on the Si porous nanospheres, revealing the formation of Si/TiO_2 Z-scheme system. The high-magnification TEM in Figure 3(d) depicts many different lattice fringes of the Si/TiO_2 nanocomposites. The fringes with lattice spacing of ca. 0.235 nm and 0.31 nm observed in the HRTEM image match those of the (001) and (111) crystallographic planes of anatase TiO_2 and Si nanoparticles, indicating the forming of Si/TiO_2 interface via a hydrothermal method, which may improve the photocatalytic properties of TiO_2.

3.2 Optical absorption properties

Figure 4(a) shows the UV-Vis absorption spectra of the Si nanospheres, TiO_2 nanosheets and direct Z-scheme Si/TiO_2 nanospheres. It can be noticed from the spectra that the as-prepared TiO_2 and Si/TiO_2 nanocomposites exhibit similar absorption behaviour in the ultraviolet region. However, Si/TiO_2 Z-scheme nanospheres show an enhanced absorbance throughout the visible light region due to the existence of Si which is a visible light responded material with a band gap of 1.12 eV. The improved visible light absorption explains the enhanced photocatalytic properties of the direct Z-scheme Si/TiO_2 nanospheres, as described later.

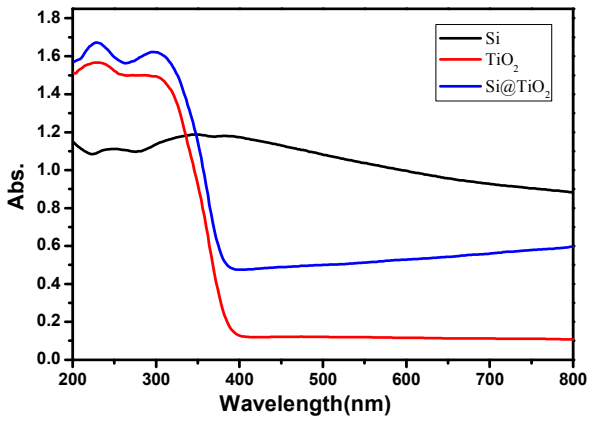

Figure 4. UV-Vis absorption spectra of Si nanospheres, TiO_2 nanosheets and direct Z-scheme Si/TiO_2 nanospheres.

3.3 Photocatalytic reduction of CO_2

To evaluate the photocatalytic activity of Si nanospheres, TiO_2 nanosheets and direct Z-scheme Si/TiO_2 nanospheres,

the conversion of CO_2 into hydrocarbon fuels in distilled water was investigated using a high power pulsed laser as light source at 355 nm wavelength. As we know, numbers of reaction products (such as HCHO, CH_3OH, HCOOH, CO, CH_4, et al) could be obtained during the CO_2 photo-reduction process. The following reactions may be the pathways of CO_2 photoreduction into value added hydrocarbons.

Catalyst + hν → $e^-_{cb} + h^+_{vb}$

$2H_2O + 4h^+ \rightarrow 4H^+ + O_2$ +0.82 V

$CO_2 + 2H^+ + 2e^- \rightarrow HCOOH$ -0.61 V

$CO_2 + 2H^+ + 2e^- \rightarrow CO + H_2O$ -0.53 V

$CO_2 + 4H^+ + 4e^- \rightarrow HCHO + H_2O$ -0.48 V

$CO_2 + 6H^+ + 6e^- \rightarrow CH_3OH + H_2O$ -0.38 V

$CO_2 + 8H^+ + 8e^- \rightarrow CH_4 + H_2O$ -0.24 V

In this study, we were selective to obtain CH_3OH as the main product of CO_2 photocatalytic reduction over Si/TiO_2 nanocomposites. Our comparative tests demonstrated that nearly no product was found by using Si nanospheres or TiO_2 nanosheets as photocatalysts. This may be due to the low conductive band potential of TiO_2 and low valance band potential of Si, respectively. The conduction band (CB) and valence band (VB) edge of Si and TiO_2 semiconductors were calculated by the equation as follows and presented in Table 1.

$$E_{CB} = X\text{-}E_C - 1/2E_g \ ^{38}$$

$$E_{VB} = E_g + E_{CB}$$

Where X is the absolute electronegativity of the semiconductor; E_C is the energy of free electrons on hydrogen scale (4.5 eV) and E_g is the band gap of the semiconductor.

It can be inferred from the table that, although the calculated VB band edge electrochemical potential of TiO_2 (2.91 V vs NHE) is high enough to initiate the reaction of H_2O and h^+ to form O_2 and H^+ (0.82 V vs NHE), the calculated CB band edge electrochemical potential (-0.29 V vs NHE) is lower than the reaction needed potential of CO_2 transforming to CH_3OH with H^+ and photogenerated e^- (-0.38 V vs NHE), resulting in the thermodynamic impossibility of CO_2 photoreduction into CH_3OH over TiO_2 catalyst under the irradiation of 355 nm laser. In the same way, pure Si catalyst has an appropriate CB band edge electrochemical potential to reduce CO_2 into CH_3OH with H^+ and e^-, but its low VB band edge electrochemical potential (0.72 V vs NHE) cannot transform any H^+ from the reaction of H_2O oxidation, which enables the photoreduction of CO_2 into CH_3OH.

Table 1. Relevant Parameters of Ti, O, Si Atoms (Ionization Energy, Atomic Electron Affinity and Absolute Electronegativity) and TiO_2, Si Semiconductors (Absolute Electronegativity, Band Gap and Electrochemical Potentials of CB/VB Band Edges)

Elements	Si	Ti	O
Atomic ionization energy (eV)	8.15168	6.82812	13.6182
Atomic electron affinity (eV)	1.38952	0.079	1.46111
Absolute electronegativity (eV)	4.7704	3.45356	7.53958
Catalysts	Si	TiO_2	
Band gap (eV)	1.1	3.2	
Absolute electronegativity (eV)	4.7706	5.81193	
CB band edge electrochemical potential (V vs. NHE)	-0.38	-0.29	
VB band edge electrochemical potential (V vs. NHE)	0.721	2.912	

The relevant data were selected from handbook[39]

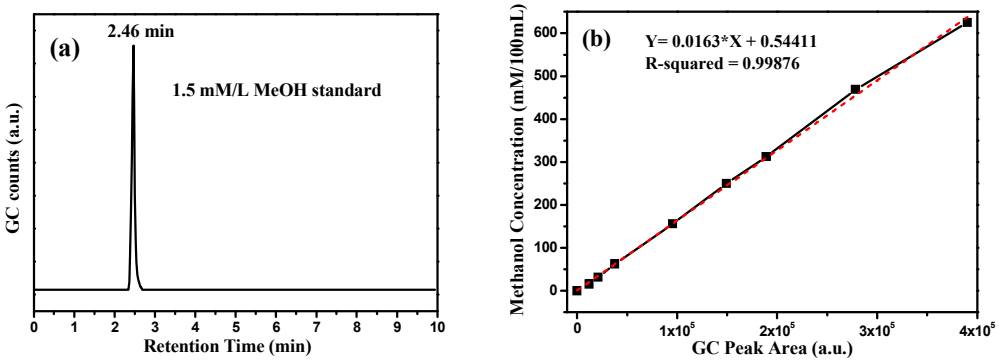

Figure 5. (a) GC peak position of methanol standard; (b) Calibration curve for methanol concentration vs GC peak area.

Gas chromatogram (GC) was employed to verify and quantify the methanol products from the CO_2 reduction over direct Z-scheme nanospheres. It is depicted in Figure 5(a) that the retention time for methanol standard is 2.46 min for the selected GC parameters and the used column. The relationship between GC peak area and methanol concentration was confirmed by using known methanol concentrations in a standard sample for calibration as depicted in Figure 5(b), which exhibits a linear trend.

Figure 6(a) depicts the GC peaks of products for samples from CO_2 photoreduction, which are taken after every 30 minutes interval of irradiation with 355 nm laser by using Si/TiO_2 as photocatalyst. It can be seen clearly that all the GC peaks in Figure 6(a) appear at exactly 2.46 min of the

retention time and no other GC peaks were detected, which suggests that the methanol is the only product obtained through the laser induced photocatalytic reduction of CO_2, possibly because of the sharp line width of the laser beam centred around 355 nm (highly monochromatic) of the pulsed laser radiation. Furthermore, it was shown that the GC peak areas of methanol from CO_2 photoreduction increase with the irradiation time (30 min, 60 min, 90 min, 120 min, 150 min) and gets the maximum in 150 min of irradiation and starts to fall. Figure 6(b) shows the concentration variation of the photocatalytic process of converting CO_2 into methanol with laser irradiation. It can be observed that the produced methanol concentration increases with the laser irradiation time and reaches its maximum (197 μM/100mL) at 150 min, but afterwards it declines. The decrease of the methanol concentration may be caused by the existence of photocatalytic oxidation effect of Si/TiO_2 composed semiconductor with positive VB position. When the methanol was produced in a substantial amount, it will be adsorbed on the surface of the photocatalysts and oxidized to inorganic matter, which is in agreement with the results obtained and explanation of other groups.[37, 40-41]

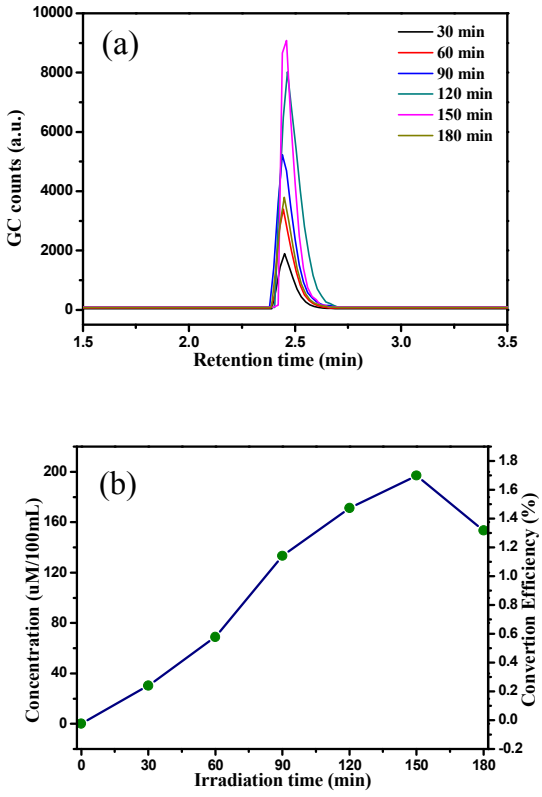

Figure 6. (a) GC peaks of methanol for sample taken after per 30 min time interval of irradiation with a laser pulse energy of 40 mJ/ pulse at 355 nm radiation with 600 mg catalyst in 100 ml distilled water, 50 PSI CO_2 pressure. (b) Concentration of produced CH_3OH and conversion efficiency with time.

In order to estimate the efficiency of CO_2 conversion into methanol using direct Z-scheme Si/TiO_2 nanospheres as photocatalyst with 355 nm laser irradiation, the process of the CO_2 conversion efficiency was estimated. The amount of CO_2 dissolved in distilled water under our experimental conditions can be calculated from Henry's law and the amount of CO_2 dissolved in 1 L water at atmospheric pressure is 34 mmol (Henry constant). As the pressure in the photocatalytic measurement is 50 psi (3.4 atm), total CO_2 dissolved in 100 ml of water is 11.56 mmol. Once we know the methanol concentration at different irradiation times of the photocatalytic process, the CO_2 conversion efficiency can be calculated from the quotient of actual concentrations of methanol and CO_2 concentration (as shown in Figure 6(b)). For that the maximum concentration of methanol is 197 μM/100mL after 150 minutes of laser irradiation, the maximum CO_2 conversion efficiency calculated (197/11560) to be about 1.71%. However, according to the Schüler's experimental result,[42] the CO_2 solubility in binary mixtures of water and methanol increases with increasing methanol content, resulting the actual CO_2 conversion efficiency slightly lower than the calculated efficiency (1.71%).

Moreover, we can calculate the photonic efficiency of the photocatalytic reduction of CO_2 from the number of methanol molecules produced for certain irradiation time and the number of consumed photons in the reaction. The number of methanol molecules can be estimated from the molar concentrations and the Avogadro number. In the case of laser, the number of photons at 355 nm wavelength with the laser pulse energy of 40 mJ/pulse and repetition rate of 10 Hz can be calculated to be 4.286×10^{19} photons/min. The maximum rate of methanol is 1.294×10^{18} molecules/min at the irradiation time interval from 60 min to 90 min. As a single methanol molecule needs 6 photogenerated electrons, the maximum photonic efficiency (P.E) of photoreduction of CO_2 can be calculated ($6\times1.294\times10^{18}/4.286\times10^{19}$) to be about 18.1%. The achievement of high photonic efficiency of direct Z-scheme Si/TiO_2 nanospheres may be due to the construction nature of Si/TiO_2 direct Z-scheme system.

3.4 Mechanism Analysis on the Enhanced Photocatalytic Activity of Si/TiO_2

As shown in Figure 7, photoluminescence spectroscopy was employed for further investigation of the photocatalytic activities of TiO_2 nanosheets and direct Z-scheme Si/TiO_2 nanospheres. Two major components of the spectrum of direct Z-scheme Si/TiO_2 nanospheres consisted of a strong peak at 540 nm and a weak, broad peak from 400 to 520 nm, which are attributed to Si and TiO_2 respectively. Moreover, it can be seen clearly that the peak intensities in photoluminescence intensity of Si/TiO_2 Z-scheme nanospheres are much lower in contrast to that of Si nanospheres and TiO_2 nanosheets. As the PL emission was resulted from the recombination of photo-induced charge carriers and information regarding the efficiency of charge carrier trapping, and their recombination kinetics can be drawn from the PL spectra,[43] it can be inferred that direct Z-scheme Si/TiO_2 nanospheres have a higher efficient separation rate of photo-generated charge carriers than that of TiO_2 nanosheets, which can be attributed to the formation of Si/TiO_2 direct Z-scheme system.

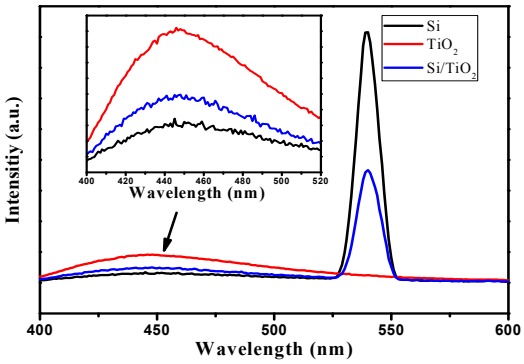

Figure 7. Photoluminescence spectra of TiO_2 nanosheets and direct Z-scheme Si/TiO_2 nanospheres.

In order to confirm the effect of Si/TiO_2 direct Z-scheme system on improving the charge separation efficiency, RhB was selected to be target pollutant for degradation by Si nanospheres, TiO_2 nanosheets and direct Z-scheme Si/TiO_2 nanospheres under 300 W Xe arc lamp irradiation with an illumination intensity of 400 mW/cm^2. As shown in Figure 8(a), it can be clearly seen that RhB molecules were completely decomposed by Si/TiO_2 direct Z-scheme nanospheres after 1 h Xe arc lamp irradiation while only 88.5% by TiO_2 nanosheets and 6.6% by Si nanospheres, which indicating an enhanced photocatalytic activity for the Si/TiO_2 Z-scheme compared with the TiO_2 nanosheets and Si nanospheres. Figure 8(b) depicts the kinetic study of photocatalytic degradation of RhB solution over the three photocatalytic materials. The linear relationship of $ln(C_0/C)$ vs irradiation time suggests that degradation of RhB is a first order reaction. The calculated rate constants for Si nanospheres, TiO_2 nanosheets and Si/TiO_2 Z-scheme nanospheres are 0.000772, 0.0354 and 0.074 min^{-1} respectively, from which it can be seen that Si/TiO_2 Z-scheme have the best photocatalytic activity which is 2.09 times of the TiO_2 nanosheets and 95.8 times of the Si nanospheres. Therefore, construction of Si/TiO_2 Z-scheme is beneficial to improve the photocatalytic activity of Si and TiO_2 extensively.

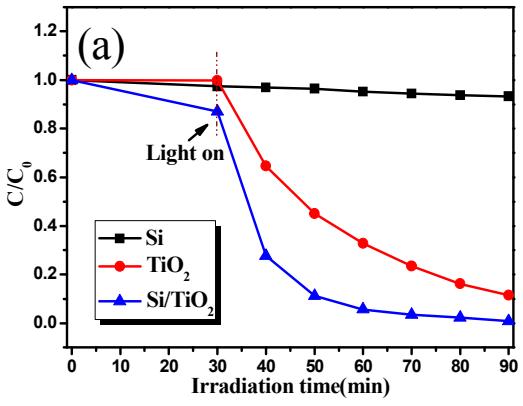

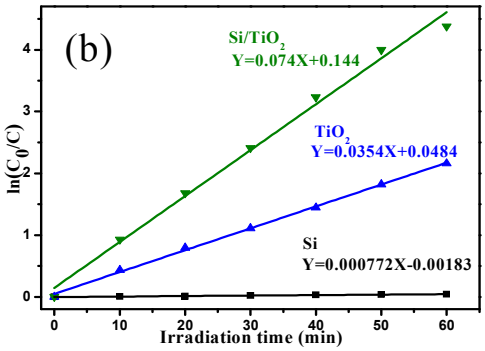

Figure 8. Photocatalytic degradation rates (a) and the $ln(C_0/C)$ vs irradiation time curves of RhB (b).

Furthermore, the CO_2 photocatalytic reduction under Xe arc lamp irradiation was carried out to investigate the influence of light source and experimental conditions on the product. Figure 9(a) shows that CO_2 can be photoreduced to CH_4 by using all the prepared samples as photocatalysts. It is obvious that direct Z-scheme Si/TiO_2 nanocomposites exhibit much higher activity than pure TiO_2 nanosheets and Si nanospheres. The higher conversion is attributed to the improved photogenerated carriers separation efficiency of Si/TiO_2 Z-scheme system. To further investigate whether CH_4 is a product of CO_2 photocatalytic reduction, we carried out a series comparative experiments to investigate the source of C and H in the produced CH_4 under Xe arc lamp irradiation. As shown in Figure 9(b), the CH_4 detected in normal condition is much higher than that in other experiments. It should be noted that the extremely low CH_4 concentrations in unnormal conditions are from the natural containing of CH_4 in the air (1-2 ppm). In other words, CH_4 can be produced only in the case of possessing all the conditions including of catalyst, CO_2, H_2O and light. It can be inferred from the contrast experiment results that, C in the photoreduction product CH_4 is from CO_2, while H is from H_2O. Therefore, it can be confirmed that the detected CH_4 is from the photoreduction of CO_2, but not a product of organic oxidation at the Si/TiO_2 Z-scheme or release of surface bound organics.

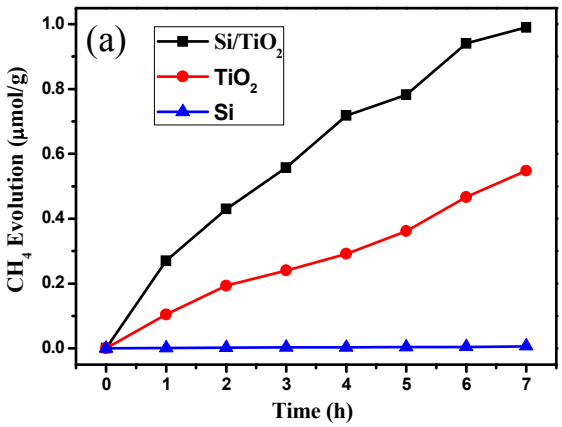

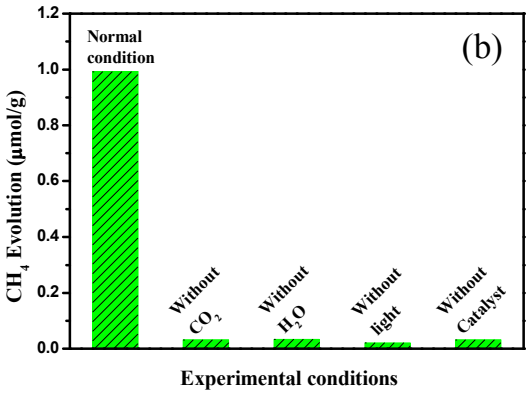

Figure 9. (a) CH_4 evolution with time under a Xe arc lamp irradiation; (b) Comparative experiments of the CO_2 photoreduction under different conditions.

Because the photocatalytic process is surface orientated, the specific surface areas of the prepared TiO_2 nanosheets and Si/TiO_2 nanocomposites were also measured by BET to study the actual exposed surface area in the photocatalytic reaction. As shown in the Figure 10, the Si/TiO_2 sample possesses a slightly higher specific surface area (165.4 m^2/g) than TiO_2 nanosheets (154.3 m^2/g) due to the surface structuring effect by the formation of spherical heterostructure with TiO_2 nanosheets well dispersed. In the photocatalytic reduction of CO_2 experiments, our results show that only the Si/TiO_2 sample is capable to produce methanol under laser irradiation for the thermodynamics cause, indicating that the exposed surface area of the catalyst has no effect on its photocatalytic reduction activity. In the photocatalytic degradation experiment, 0.1 g of the as-prepared Si, TiO_2 and Si/TiO_2 catalysts was adopted, respectively. The slightly difference of the catalysts in specific surface area is as small as 6.6 percent, which is supposed not to be the main reason for the great improvement of photodegradation efficiency (more than twice). Hence, it can be concluded that the excellent performance of Si/TiO_2 catalyst is not resulting from surface structuring effect, but the improved photo-generated carriers' concentration and separation efficiency beneficial from the Si/TiO_2 direct Z-scheme system construction.

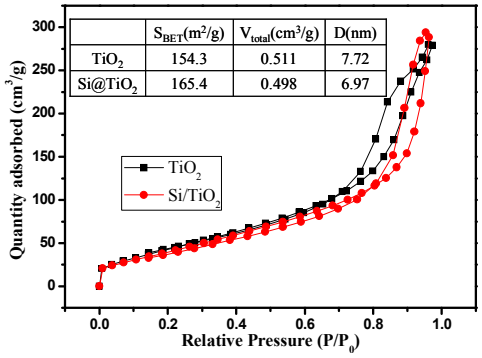

	$S_{BET}(m^2/g)$	$V_{total}(cm^3/g)$	D(nm)
TiO_2	154.3	0.511	7.72
$Si@TiO_2$	165.4	0.498	6.97

Figure 10. N_2 adsorption-desorption isotherms of TiO_2 nanosheets and direct Z-scheme Si/TiO_2 nanospheres.

Figure 11 illustrates the schematic charge flow in Si/TiO_2 direct Z-scheme system under illumination. 355 nm lasers can be harvested by both Si and TiO_2 to generate e^-/h^+ pairs. As reported in Yang's previous research,[32] the photogenerated hole in TiO_2 ($_{TiO_2}h^+$) move toward the TiO_2/electrolyte interface and oxidizes OH^- to oxygen, while photogenerated electrons in the TiO_2 ($_{TiO_2}e^-$) move away from the interface between TiO_2 and the electrolyte due to the schottky barrier. The potential barrier at the Si/TiO_2 interface reflects holes back into the TiO_2 layers. To complete the circuit, the photogenerated electrons in Si ($_{Si}e^-$) move to the surface where the CO_2 reduction reaction takes place. The photogenerated hole in Si ($_{Si}h^+$) moves towards the Si/TiO_2 interface and recombines with the $_{TiO_2}e^-$. Therefore, the direct Z-scheme Si/TiO_2 nanospheres show high activity towards CO_2 reduction into methanol since its band alignment at the junction helps reduce recombination under illumination. However, for individual Si photacatalyst, its VB potential (+0.721 V vs NHE) is not high enough to achieve the oxidation reaction potential (O_2/H_2O 0.82 V Vs NHE). Similarly, the CB potential of TiO_2 (-0.29 V vs NHE) is too low to initiate the CO_2 reduction reaction into methanol (CH_3OH/CO_2 -0.38 V Vs NHE). In other words, the individual Si nanospheres or TiO_2 nanosheets lack suitable VB or CB potential to photoreduce CO_2 into methanol.

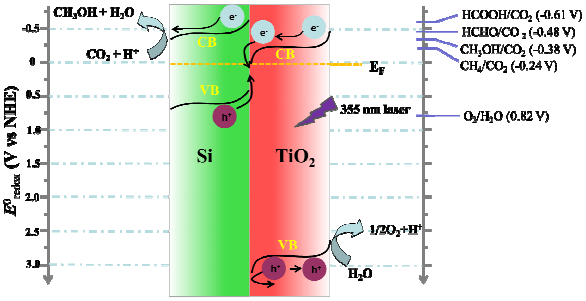

Figure 11. Schematic diagram of enhanced photocatalytic property in the Si/TiO_2 direct Z-scheme system for CO_2 reduction.

4. Conclusion

In summary, we have presented a facile and low cost method to prepare direct Z-scheme Si/TiO_2 nanostructure via hydrothermal reaction with tetrabutyl titanate and Si powder which was prepared from the magnesiothermic reduction of SiO_2 stöber nanospheres. All the results indicate that Si/TiO_2 nanocomposites possess much higher photocatalytic activity than individual Si and TiO_2 samples for the CO_2 conversion and degradation of RhB. This excellent performance could be attributed to the integrated suitable conductive band of Si and valence band of TiO_2 for CO_2 reduction and improved light absorption ability, enhanced concentration of photo-generated carriers, and higher separation efficiency due to the elaborate construction of Si/TiO_2 direct Z-scheme system.

Acknowledgments

This work was financially supported by the National Natural Science Foundation of China (No. 51172109), the Fundamental Research Funds for the Central Universities (NO: NS2014057), Funding of Jiangsu Innovation Program for Graduate Education (No. CXLX12_0148), and the

Fundamental Research Funds for the Central Universities. This work is also supported by KFUPM through project # RG1011-1/2.

Notes and references

[a]*College of Materials Science and Technology, Nanjing University of Aeronautics and Astronautics, Nanjing 210016, P. R. China.*
[b]*Physics Department, King Fahd University of Petroleum and Minerals, Dhahran, 31261, Saudi Arabia.*
**Corresponding author, a*Prof. Guangbin Ji, Tel.: +86-25-5211-2902. E-mail: gbji@nuaa.edu.cn; b*Prof. Mohammed Ashraf Gondal, Tel.: +966-38602351, Email: magondal@kfupm.edu.sa.*

1. C. J. Wang, O. Ranasingha, S. Natesakhawat, P. R. Ohodnicki, M. Andio, J. P. Lewis, C. Matranga. *Nanoscale* 2013, **5**, 6968-6974.
2. F. C. Meunier. *Angew. Chem. Int. Ed.* 2011, **50**, 4053-4054.
3. Y. S. Chaudhary, T. W. Woolerton, C. S. Allen, J. H. Warner, E. Pierce, S. W. Ragsdale, F. A. Armstrong. *Chem. Commun.* 2012, **48**, 58-60.
4. S. C. Yan, S. X. Ouyang, J. Gao, M. Yang, J. Y. Feng, X. X. Fan, L. J. Wan, Z. S. Li, J. H. Ye, Y. Zhou, Z. G. Zou. *Angew. Chem. Int. Ed.* 2010, **49**, 6400-6404.
5. Q. Liu, Y. Zhou, J. H. Kou, X. Y. Chen, Z. P. Tian, J. Gao, S. C. Yan, Z. G. Zou. *J. Am Chem. Soc.* 2010, **132**, 14385-14387.
6. N. Zhang, S. X. Ouyang, T. Kako, J. H. Ye. *Chem. Commun.* 2012, **48**, 1269-1271.
7. P. Q. Wang, Y. Bai, P. Y. Luo, J. Y. Liu. *Catal. Commun.* 2013, **38**, 82-85.
8. T. Wang, X. G. Meng, P. Li, S. X. Ouyang, K. Chang, G. G. Liu, Z. W. Mei, J. H. Ye. *Nano Energy* 2014, **9**, 50-60.
9. S. S. Tan, L. Zou, E. Hu. *Catal. Today* 2006, **115**, 269-273.
10. O. Ozcan, F. Yukruk, E. U. Akkaya, D. Uner. *Top. Catal.* 2007, **44**, 523-528.
11. K. R. Thampi, J. Kiwi, M. Graetzel. *Nature* 1987, **327**, 506-508.
12. A. L. Linsebigler, G. Q. Lu, J. T. Yates. *Chem. Rev.* 1995, **95**, 735-758.
13. Hussain S. T.; Khan K.; Hussain R. *J. Nat. Gas Chem.* 2009, **18**, 383-391.
14. O. K. Varghese, M. Paulose, T. J. Latempa, C. A. Grimes. *Nano Lett.* 2009, **9**, 731-737.
15. J. G. Yu, G. P. Dai, Q. J. Xiang, M. Jaroniec. *J. Mater. Chem.* 2011, **21**, 1049-1057.
16. K. Koci, L. Matejova, L. Obalova, S. Krejckov, Z. Lacny, D. Placha, L. Capek, A. Hospodkovad, O. Solcova. *Appl. Catal. B: Environ.* 2010, **96**, 239-244.
17. W. B. Hou, W. H. Hung, P. Pavaskar, A. Goeppert, M. Aykol, S. B. Cronin. *ACS Catal.* 2011, **1**, 929-936.
18. K. P. Yu, W. Y. Yu, M. C. Kuo, Y. C. Liou, S. H. Chien. *Appl. Catal. B: Environ.* 2008, **84**, 112-118.
19. Y. Li, W. N. Wang, Z. Zhan, M. H. Woo, C. Y. Wu, P. Biswas. *Appl. Catal. B: Environ.* 2010, **100**, 386-392.
20. C. J. Wang, R. L. Thompson, P. Ohodnicki, J. Baltrus, C. Matranga. *J. Mater. Chem.* 2011, **21**, 13452-13457.
21. S. Qin, F. Xin, Y. Liu, X. Yin, W. J. Ma. *Colloid Interface Sci.* 2011, **356**, 257-261.
22. Q. D. Truong, J. Y. Liu, C. C. Chunq, Y. C. Ling. *Catal. Commun.* 2011, **19**, 85-89.
23. P. Zhou, J. G. Yu, M. Jaronniec. *Adv. Mater.* 2014, **26**, 4920-4935.
24. H. Tada, T. Mitsui, T. Kiyonaga, T. Akita, K. Tanaka. *Nat. Mater.* 2006, **5**, 782-786.
25. H. Lin, J. Cao, B. Luo, B. Xu, S. Chen, *Catal. Commun.* 2012, **21**, 91-95.
26. Z. B. Yu, Y. P. Xie, G. Liu, G. Q. Lu, X. L. Ma, H. M. Cheng, *J. Mater. Chem. A* 2013, **1**, 2773-2776.
27. J. G. Yu, S. H. Wang, J. X. Low, X. Wei. *Phys. Chem. Chem. Phys.* 2013, **15**, 16883-16890.
28. M. Miyauchi, Y. Nukui, D. Atarashi, E. Skai. *ACS Appl. Mater. Interfaces* 2013, **5**, 9770–9776.
29. Y. C. Wang, J. Tang, Z. Peng, Y. H. Wang, D. S. Jia, B. Kong, A. A. Elzatahry, D. Y. Zhao, G. F. Zheng. *Nano Lett.* 2014, **14**, 3668-3673.30. M. W. Shao, L. Cheng, X. H. Zhang, D. D. D. Ma, S. T. Lee. *J. Am. Chem. Soc.* 2009, **131**, 17738-17739.
31. N. Megouda, Y. Cofininier, S. Szunerits, T. Hadjersi, O. ElKechai, R. Boukherroub. *Chem. Commun.* 2011, **47**, 991-993.
32. Y. J. Hwang, A. Boukai, P. D. Yang. *Nano Lett.* 2009, **9**, 410-415.
33. J. Shi, X. D. Wang. *Energy Environ. Sci.* 2012, **5**, 7918-7922.
34. Q. D. Wu, D. Z. Li, Z. X. Chen, X. Z. Fu. *Photochem. Photobiol. Sci.* 2006, **5**, 653-655.
35. C. Liu, J. Y. Tang, M. Chen, B. Liu, P. D. Yang. *Nano Lett.* 2013, **13**, 2989-2992.
36. W. Stöber, A. Fink, E. J. Bohn. *J. Colloid Interface Sci.* 1968, **26**, 62-69.
37. M. A. Gondal, M. A. Ali, X. F. Chang, K. Shen, Q. Y. Xu, Z. H. Yamani. *J. Environ. Sci. Health., Part A* 2012, **47**, 1571-1576.
38. X. F. Chang, J. Huang, C. Cheng, Q. Sui, W. Sha, G. B. Ji, S. B. Deng, G. Yu. *Catal. Commun.* 2010, **11**, 460-464.
39. D. R. Lide. Handbook of Chemistry and Physics, 87th ed. Florida: CRC Press, 2006-2007.
40. S. Suzuki, T. Tsuneda, K. Hirao. *J. Chem. Phys.* 2012, **136**, 024706(1-6).
41. C. Y. Wang, J. Rabani, D. W. Bahnemanna, J. K. Dohrmann. *J. Photochem. Photobiol. A: Chem.* 2002, **148**, 169-176.
42. N. Schüler, K. Hecht, M. Kraut, R. Dittmeyer. *J. Chem. Eng. Data.* 2012, **57**, 2304-2308.
43. L. Q. Jing, Y. C. Qu, B. Q. Wang, S. D. Li, B. J. Jiang, L. B. Yang, W. Fu, H. G. Fu, J. Z. Sun. *Sol. Energ Mater. Sol. Cells* 2006, **90**, 1773-1787.

High-Active Si/TiO_2 Heterojunction Photocatalyst for Boosted CO_2 Reduction into Value-added Methanol

Yousong Liu [a], Guangbin Ji [a*], Mohammed Abdulkader Dastageer [b], Lei Zhu [a], Junyi Wang [a], Bin Zhang [a] and Xiaofeng Chang [a] and Mohammed Ashraf Gondal [b*]

[a]*College of Materials Science and Technology, Nanjing University of Aeronautics and Astronautics, Nanjing 210016, P. R. China.*
[b]*Physics Department, King Fahd University of Petroleum and Minerals, Dhahran, 31261, Saudi Arabia.*
**Corresponding author, a*Prof. Guangbin Ji, Tel.: +86-25-5211-2905. E-mail: gbji@nuaa.edu.cn; b*Prof. Mohammed Ashraf Gondal, Tel.: +966-38602351, Email: magondal@kfupm.edu.sa.*

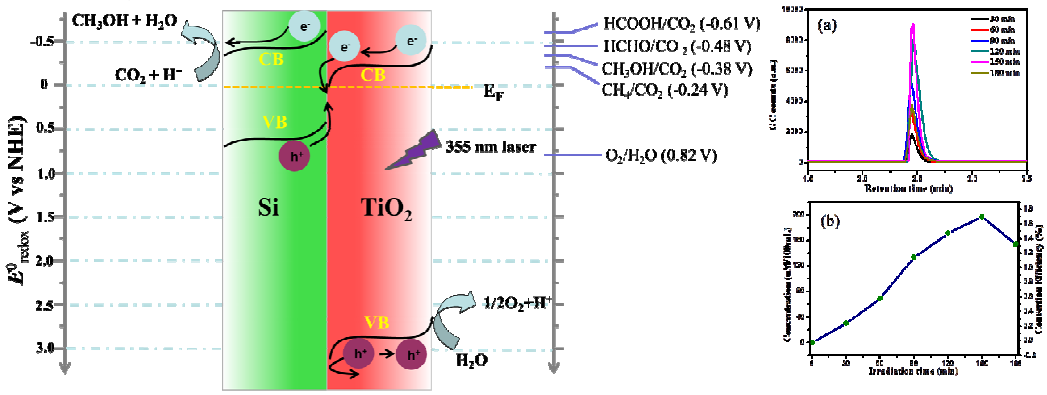

Si/TiO_2 heterojunction photocatalyst was synthesized via a facile hydrothermal reaction using tetrabutyl titanate and Si powder. CO_2 photocatalytic reduction proved that Si/TiO_2 nanocomposites exhibit high activity in conversion of CO_2 to methanol with the maximum photonic efficiency of 18.1%, while pure Si and TiO_2 catalyst are almost inactive, which can be ascribed to the integrated suitable band composition and improved photo-generated carriers' separation efficiency in the Si/TiO_2 heterojunction for CO_2 reduction under laser irradiation.